coatings

MDPI

Article

Superhydrophobic Coatings from Recyclable Materials for Protection in a Real Sea Environment

Michele Ferrari *, Alessandro Benedetti and Francesca Cirisano

CNR-ICMATE National Research Council, Institute of Condensed Matter Chemistry and Technologies for Energy, Via De Marini, 6, 16149 Genova, Italy; alessandro.benedetti@ge.icmate.cnr.it (A.B.); francesca.cirisano@ge.icmate.cnr.it (F.C.)

* Correspondence: michele.ferrari@ge.icmate.cnr.it

Received: 10 April 2019; Accepted: 2 May 2019; Published: 6 May 2019

Abstract: Recyclable materials can be referred to as both those materials directly recycled from wastes and those derived from any kind of transformation before use. Highly water repellent coatings with wettability properties, known as superhydrophobic (SH), are related to surfaces with contact angles above 150° and a very small hysteresis. The small area available for these surfaces when in contact with water can be exploited in many applications in which interactions with an aqueous environment are usually desirable to be avoided, like for protection and friction reduction in a marine environment. SH coatings under investigation have been prepared starting from recyclable materials with the aim to provide a sustainable and low cost solution, with potential application to large surfaces in a marine environment. Wetting studies, surface characterization, and electrochemical tests show how these surfaces can be used in terms of fouling prevention and the protection of metals in underwater conditions.

Keywords: superhydrophobic; sustainable materials; marine environment; fouling; corrosion

1. Introduction

Protecting metals from corrosion by means of superhydrophobic (SH) coatings can be regarded as a promising technological breakthrough, because of the reduced area available for water in contact with solid, allowing metal substrates' interactions with aqueous corrosive species to be minimized, providing superior anticorrosive performances. Among the preparation methods proposed, most are not suitable for larger surfaces, being only laboratory-scaled and not yet of potential interest for real applications. This limitation mainly lies in the complexity of hierarchical micro/nanostructures and costs of low surface energy materials and, from another side, their lifetime, which allows long-lasting corrosion resistance [1]. On the basis of the lotus leaf effect, nevertheless, the preparation of an SH surface has, in some case, the advantages of being a low cost solution and having the potential to be scaled-up for use over different substrates. The research on repellent materials for water and aqueous electrolytes solutions focuses on hydrophobicity and superhydrophobicity as key parameters for anti-icing, bio-corrosion, and fouling control [2].

The recent method of Huang et al. [3] deals with the preparation of an SH composite coating involving styrene copolymers, methyl methacrylate, and silica nanoparticles, previously modified with hexamethyldisilazane. The presence of silica coupled with low cost materials makes this procedure suitable for the large-scale fabrication of SH coatings for metal protection. Electrochemical and wettability studies investigated the corrosion resistance of a multi-layer composite SH coating on carbon steel in sterilized seawater composed of Ni–P, TiO_2/ZnO, and octadecyltrimethoxysilane (ODS) molecules. Electrochemical impedance spectroscopy (EIS) and polarization curves showed the

efficiency of a bi-layer or three-layer composite coating on carbon steel in improving the corrosion resistance in sterilized seawater [4].

An SH composite coating with high adhesion strength was employed to enhance for both heat dissipation and anti-corrosion. Plasma electrolytic oxidation followed by electrodeposition resulted in an Al_2O_3/cerium hexadecanoate (Al_2O_3/CH) system with excellent water repelling and self-cleaning ability, owing to the micro/nano structure and low surface energy. The composite coating enhances the corrosion potential of pure Al, lowering the corrosion current density by two orders of magnitude, and drops the operation temperature of a lamp by almost ten degrees [5].

Metal corrosion in industrial fields, like in desalination and crude oil pipelines, ship building, heat exchangers, and so on, implies high service and maintenance costs [6]; nevertheless, as in the following, many works on corrosion resistance are usually based on experiments in NaCl solutions only and for short periods considering the potential time scale to which they should have to be exposed to.

In the work of [7], an innovative SH system using an electroplating method has been introduced as a high corrosion resistance solution in an industrial environment. On the basis of inherently corrosion resistant Zn−Ni and Zn−Co alloys, the coating kept its properties after immersion into a NaCl solution for 48 h in comparison with SH NiO/ZnO and ZnO coatings, which lost the superhydrophobicity, demonstrating high corrosion potential and low corrosion density.

The research on easy and low budget fluorine-free anticorrosion SH surfaces for Al materials is still a challenge for service performance and safety. In this direction, a facile preparation of non-fluorinated *Allium giganteum*-like SH aluminium surfaces via a one-step electro-deposition approach was proposed in the work of [8], providing, beyond surface analysis and wettability, electrochemical impedance study to reveal the corrosion resistance and inhibition efficiency, in both air and 3.5 wt.% NaCl immersion tests, but in a quite short observation time window.

Another simple, but efficient solution with a longer test time has been proposed in the work of [9], where an SH coating was prepared by modifying a previously treated surface by stearic acid using the boiling water method. Electrochemical coating characterization was carried out by potentiodynamic polarization, and long-term corrosion tests were performed by immersion in NaCl solution for three months, after which a fair superhydrophobicity was maintained.

A perfluorodecyltrichlorosilane modifier (FAS) was employed in the work of [10] to hydrophobize at a low cost the micro/nano structures prepared on 5A05 Al alloy by a facile one-step immersion process. In this work, the ease of the method is claimed to be promising for applications in an ocean environment; although they have been carried out in an NaCl solution only, the stability has not been proven over a suitable length of time.

One of the most recent trends in corrosion protection is presented in the work of [11]. It consists of an underwater superoleophobic system (HN/ER-coating) based on MPS (methacryloxy propyl trimethoxyl silane)-SiO_2/PNIPAM (N-isopropylacryamide) hybrid nanoparticles and epoxy resin (ER) and has been proposed using a simple solution-casting method. The robustness of this solution has been tested under different conditions covering harsh environments or bacterial biofilm formation resulting in good performance, but again at short time scale (less than one week) for potential practical applications.

In the work of [12], the combination of an inhibitor agent and a hydrophobizing agent (cerium chloride and myristic acid, respectively) has been applied to provide an SH solution against corrosion in pipeline systems. Here, seawater is considered as an artificial mixture of NaCl and tannic acid solutions, where the carbon steel samples have been characterized in a month time window, demonstrating an improved corrosion resistance of the coated over the uncoated sample, despite an increasing weight loss with time.

In a recent work [13], a series of SH nanocomposites were prepared by solution casting using different amounts of nano-magnetite fillers, aiming to prepare a foul release (FR) paint. The samples have been tested over a longer period of time (three months) in real seawater, as well as with the assessment of growth inhibition of microorganisms like diatoms.

To the best of our knowledge, only few reference data are available [7,14–16] about superhydrophobic surfaces in real seawater environments in a time window greater than days. Furthermore, in these works, no recyclable materials have been used. Only recently have superhydrophobic properties from recyclable materials been under investigation, but not as of yet in marine environments; moreover, such materials require an additional final functionalization to improve hydrophobicity [17–19].

Following this purpose, a study of SH coatings tested in natural seawater is presented here. In particular, a low cost procedure starting from hydrophobic recyclable materials like polystyrene (PS) and polytetrafluoroethylene (PTFE) and green solvent to produce a coating with SH behaviour by the spray technique on Al substrate and glass is evaluated in terms of exposition in shallow natural seawater for a period up to two months. The combination of the PTFE chemical inertia and low surface energy and friction coefficient with the barely hydrophobic, but large availability of PS results in a sustainable highly hydrophobic solution for fouling and corrosion control purpose in a real marine environment.

2. Materials and Methods

2.1. Materials and Surface Characterization

The superhydrophobic coating was prepared based on a polytetrafluoroethylene (PTFE)–polystyrene (PS) dispersion in Ethyl Acetate (EtOAc). PS (surface tension of 40 mN/m) was obtained from recycled commercial packaging and ethyl acetate (EtOAc) and PTFE (surface tension of 20 mN/m) was purchased by Sigma-Aldrich (St. Louis, MO, USA). High purity grade water, produced by a MilliQ (Milli-Pore, Elix plus Milli-Q, Burlington, VT, USA) ion-exchange purifier with microfiltration stage (18 MΩ cm), was utilised for contact angle (CA) measurements. Pure water surface tension was measured by a PAT-1 tensiometer (Sinterface, Berlin, Germany) at 20 °C stable for several hours at 72.5 ± 0.2 mN/m. The use of EtOAc as "green solvent" is not intended as a recycled material, but as a very low toxicity solvent in line with the general overview of the project to produce highly performance materials from sustainable and environmental friendly substances.

The superhydrophobic surface was produced by spray coating the PTFE–PS dispersion at room temperature and atmospheric conditions on a suitable substrate. For the purpose of this study, glass was used as a substrate (owing to its inertia with respect to the performed test) in the first campaign, and commercial aluminium alloy 5754 H111 (Al–5% Mg alloy) was used for the second campaign, as already done in our previous work with different SH coating composition and surface morphology not coming from recyclable materials [20]. More details regarding the first and second campaigns are provided successively.

For both campaigns, no primer was used, in order to observe the adhesion of the coatings under the stress imposed by the biology without the interfering substrate, but probably enhancing the adhesion and performance. In order to evaluate the wetting behaviour of the samples, before and after the immersion test, contact angle (CA) was acquired using an ASTRA view tensiometer (developed at CNR–ICMATE, Genoa, Italy [21]) at room temperature. The CA was measured in at least three different points of the surface. The samples' surface was furthermore characterised before and after test by different techniques; namely, scanning electron microscopy (SEM) (LEO 1450VP, LEO Electron Microscopy Ltd., Cambridge, UK), light optical microscopy (LOM) (Zeiss-AXIO), and 3D confocal and interferometric profilometry (Sensofar S-NEOX, Barcelona, Spain). The 3D profilometry was chosen to obtain surface parameters for its ease of use and because it allows larger surface scans. The surface characterisation by profilometry was done according to the standard ISO 25178 [22].

In particular, for this study, surface roughness (*Sa*), an amplitude parameter, and void volume (Vv), a functional parameter, were investigated. *Sa* is a very general and commonly used parameter in practical applications and is given in nm or µm, Vv instead is not commonly used in association with the surface study regarding wettability. Vv is related to the distribution of heights and its cumulated curve (called the Abbott–Firestone curve), and is aimed at characterizing the functional behaviour of the

surface, such as wear, lubrication, and contact. This parameter is the volume of the voids at a material ratio p (in %) and is given in $\mu m^3/\mu m^2$. In Figure 1, the Abbott–Firestone curve is presented with all parameters related to the volume, included the void volume (Vv). This parameter was considered because of its nature, being related to the concept of entrapped air, describing the superhydrophobicity (Cassie–Baxter model [23,24]), which is connected to the biofouling control of immersed SHS.

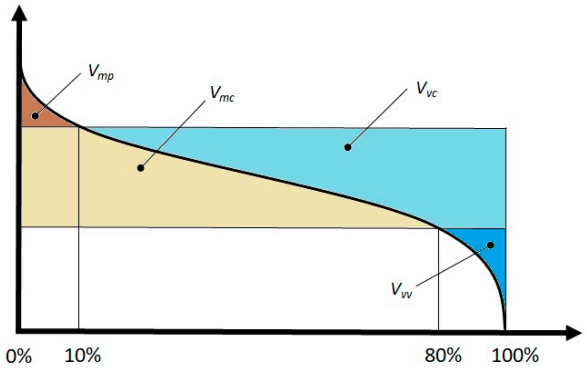

Figure 1. Graphical representation of the volume parameters with respect to the Abbott–Firestone curve.

2.2. Exposure Environments and Exposition

Immersion tests were conducted in the sea marine station of ICMATE CNR in Bonassola (80 km east Genoa in Italy, Mediterranean Sea). The investigations were performed in summer/autumn in two different campaigns.

The immersion environments were 200 L mesocosm exposed to the natural photoperiod fed with circulating natural seawater as slowly as to reduce the convection to a minimum (5 L/min). During the investigated period, the water temperature ranged from 22 °C at the beginning, progressively dropping to 20 °C near the end of the exposition period.

In both campaigns, the samples were immersed at the depth of about 10 cm with an angle of 180° (coating face down with respect to the solar irradiation). This angle was chosen after the results were obtained from the test performed in the previous campaign on the fluoropolymer coating [24]. During the whole investigation period, macroscopic images of the superhydrophobic (SH) surfaces were taken with at a weekly periodicity with a Nikon D800 camera (Nikon Corporation, Tokyo, Japan). A mirror was used to photograph surfaces while leaving the samples undisturbed in their initial position.

The first campaign, divided into two summer–autumn sessions, was done with the aim to study the behaviour of new SH coatings against fouling colonization.

To study the fouling growth, the samples, in both sessions, were immersed in natural seawater exposed to sunlight for 28 days—a period already tested in our previous work [25], long enough to observe biofouling growth and coating degradation.

The purpose of this test was also the study of the degree of biofouling coverage in relation to the surface roughness of the coatings. From the test performed in our previous work [16], fouling growth was limited by the gases entrapped in the SHS, dissolved gases coming from the presence of biology and living systems, that is, O_2 and CO_2. In particular, with time, these gases tend to coalesce in bubbles. During the first session, the immersed samples were photographed after 10 and 20 days, and after extraction and cleaning after 28 days. The samples' observation during the immersion was important because it allowed us to see the extension of the bubbles and their time evolution. The second session, performed on the same SH PS/PTFE coating, was done in autumn to deepen and confirm the trend observed in summer.

The second summer–autumn campaign on SH PS/PTFE, lasting two months, was carried out with the aim to preliminarily evaluate the new SH coating anti-corrosion behaviour. All the samples (SHa, SHb, SHc) used in this test were prepared with the same protocol with an average roughness of 6.5 μm.

At the same time, the bubbles' coalescence evolution under immersion conditions was periodically monitored (Figure 2).

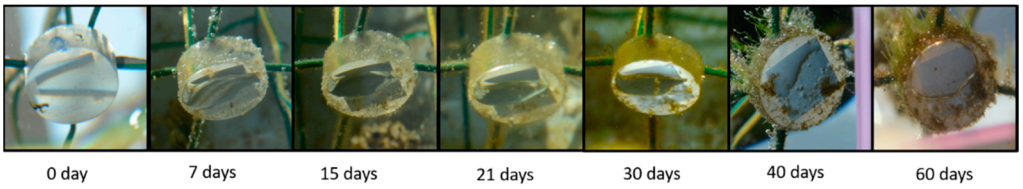

Figure 2. Image sequence of bubble formation over the observation period.

2.3. Potentiodynamic Test

Potentiodynamic scans were performed at the end of the second campaign on Al alloy samples (2 cm × 2 cm) coated with SH coating (SHa, SHb, SHc) and on a bare Al alloy sample as a control. Electrodes were embedded into epoxy resin, making only the functionalized (metal and coating) surface available for seawater interaction. The SH coated electrodes were bound onto a plastic holder such that the SH surface was turned to the bottom of the tank. A couple of samples without the SH coating as controls were placed too.

Polarization sweeps were performed on the samples in natural seawater mesocosms after 60 days of immersion, reading the current at the end of 20 s steps of 10 mV, thus resulting in a 0.5 mV/s scan speed. The reference electrode (Ref.) was Ag/AgCl and the counter electrode was Pt.

3. Results

3.1. Surface Characterization

Before the immersion test, each prepared sample was characterized by drop shape tensiometry to obtain the contact angle, and by 3D confocal and interferometric profilometry to measure the surface roughness. These measurements revealed that every sample was superhydrophobic, with CA greater than 150° and hysteresis less than 5°, and such properties were found in a large range of roughness, as reported in Figure 3.

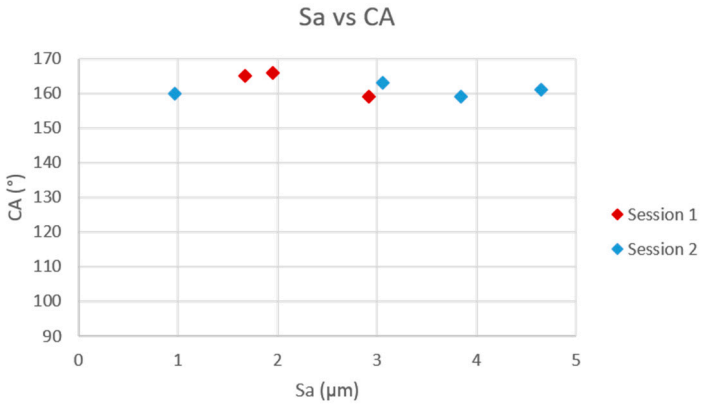

Figure 3. Contact angle (CA) of the samples of the two session with respect to surface roughness (Sa) before immersion. Red dots—session 1, blue dots—session 2.

The surface roughness of each samples was acquired before and after the immersion test. At the end of the test, *Sa* was measured only on the portion of coating without fouling to study the wear of the SH coating. As an example, in Figure 4, profilometer images of a sample used for the corrosion campaign are reported. Before immersion, *Sa* was 6.5 ± 0.2 µm; after extraction and weak pressure cleaning, *Sa* was 5.9 ± 0.2 µm. Furthermore, the portions of coating under the bubbles and after

polarization test remain superhydrophobic with CA greater than 150° and hysteresis less than 5° despite of the slight change in roughness.

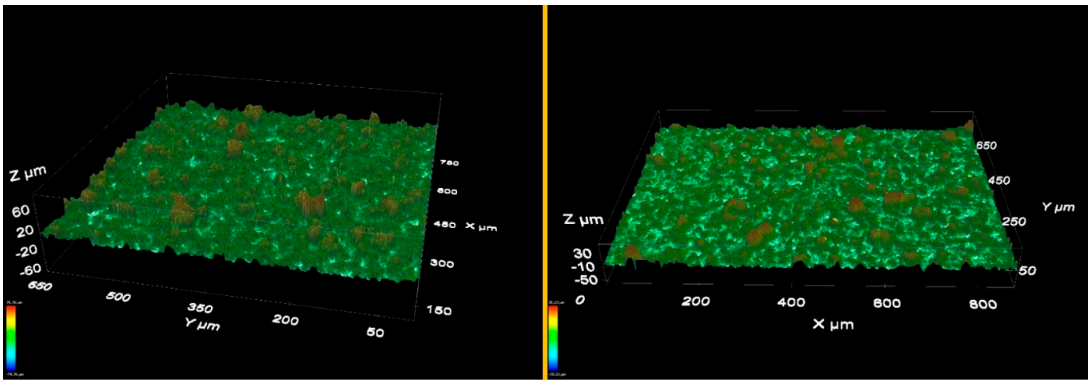

Figure 4. Three-dimensional (3D) profilometer images of a sample used for the corrosion campaign. Left—before immersion, right—after immersion.

3.2. Fouling Control Properties

The fouling control properties were studied during two different immersions in summertime and samples were photographed three times; that is, after 10 and 20 days during the immersion, and after 28 days when they were extracted and cleaned. In general, after 28 days of immersion, a soft and non-homogeneous fouling layer was grown on all immersed samples. In Figure 5, images of all immersed samples after 10 days are reported.

Figure 5. Pictures acquired at day 10 of immersion relative with different surface roughness: (**A**) *Sa* = 1.67 µm, (**B**) *Sa* =1.95 µm, (**C**) *Sa* = 2.92 µm. Scale bar under each sample is 10 mm.

It is possible to observe the different extension of the bubbles with respect to the roughness difference: in particular, the higher the *Sa*, the larger the bubble extension. Analysing the system, *Sa* seems to be directly correlated to the bubble volume. During these tests, a cleaned glass as a reference was immersed. In Figure 6, the control and SH sample are reported after 10 days of immersion.

From Figure 6, it is possible to observe that, also under the glass control, numerous bubbles developed, but with differences in number and dimensions. Here, they were very small and circular, while on the SHS bubbles, they were larger and oblate. In particular, the lateral view evidenced differences between the bubbles in the two cases: under the glass control, they were perfectly round and the air prevented the glass surface from being wetted; whereas under the SHS, the bubbles were oblate and pinned at the surface, and air spreads on the SHS, with which it is in contact.

At the end of the campaign, the samples were extracted and half cleaned by weak water pressure. After cleaning, it was observed that, in the presence of bubbles, the surface appeared without visible macrofouling compared with those areas where they were absent or too small and those where biofouling has grown. CA measurements performed on the cleaned part of the coating revealed that the surface preserved its superhydrophobicity.

Other important observation was about the adhesion of the coating on the substrate. Where the coating was covered by biofouling and when it was cleaned, it was detached and carried away, leaving the glass surface. Conversely, where the bubble protected the surface from the fouling, the pressure of

the water was not sufficient to remove the coating. These observations mean that the SH coating had a good adhesion with the glass substrate as long as it was not colonized by biofouling.

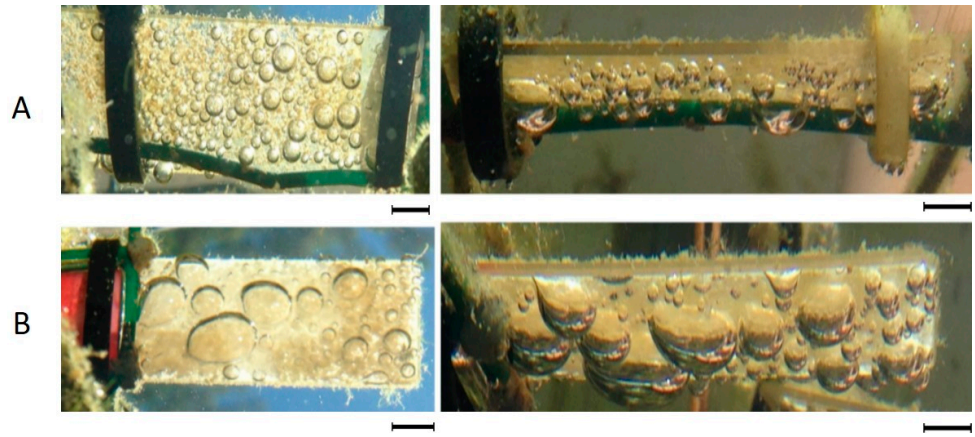

Figure 6. Glass control (**A**) and superhydrophobic (SH) sample (**B**) after 10 days of immersion. On the right side, lateral views of the bubble are reported. Scale bar under each sample is 10 mm. (Appendix A Table A1 for supporting information).

Session 2 was performed on different roughness superhydrophobic PS/PTFE samples to deepen and confirm the trend observed in the previous session. In Figure 7, all samples on the 10th day of immersion and after extraction are reported.

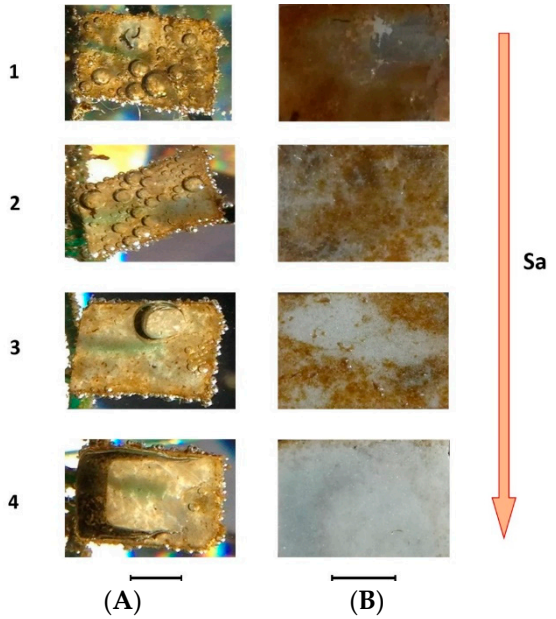

Figure 7. Superhydrophobic samples of session 2 during immersion (**A**) and after extraction (**B**). Scale bar under each column is 10 mm.

On the left side of the Figure 7, it is possible to observe the bubbles' volume, and it is evident that their extension increases with samples roughness. On the right side of the figure, samples after extraction are reported. Some of those present parts of the coating are not affected by biofouling. Comparing the images before and after extraction, it is possible to affirm that where a large bubble was present, biofouling growth was inhibited or delayed.

The evidence of fouling growth inhibition was investigated by optical microscopy and SEM analysis in order to evaluate the real foul control behaviour due to the presence of bubbles on samples

at the end of the exposition. In Figure 8, an LOM image at 5× and 20× of PS/PTFE sample is shown. At low magnification, it is already possible to distinguish the part of the sample that was covered by bubbles.

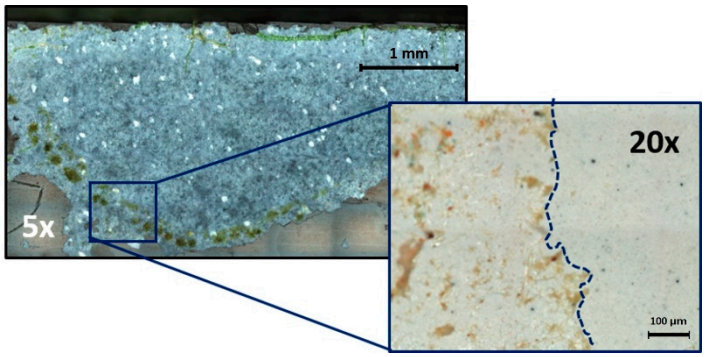

Figure 8. Optical images at 5× and 20× of the immersed coating. The photos were taken in a part of coating that was under a bubble. In particular, the 20× image was taken on the edge of the bubble.

To understand if the coating was intact under the bubble, SEM observation was performed. Figure 9 was taken on a bubble edge, distinguishing two different zones: on the left part of the image, where the bubble was present, diatoms and biomaterial attachment were prevented, while they were present on the right-lower side of the picture.

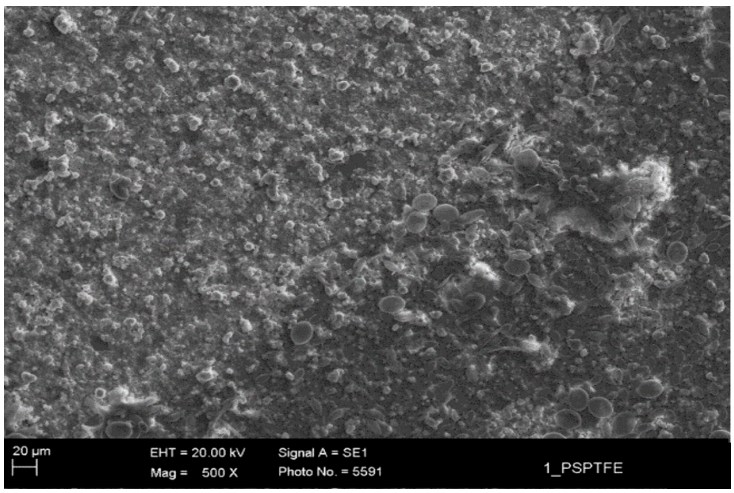

Figure 9. Scanning electron microscopy (SEM) image at 500× of recycled polymer coating in a zone at the border of the bubble; the left-upper side of the image was under the bubble.

A similar observation was carried out by 3D profilometer, taking images on the bubble edge. In Figure 10, it is possible to observe the presence of biofouling on the portion of the surface not covered by the bubble, instead of a clean surface where the bubble was present. Furthermore, an analysis on the clean part evidenced that there was not a significant loss of material in terms of *Sa*.

To better understand the correlation between bubbles and biofouling inhibition, the percentage of the clean part was calculated on samples of both sessions. To obtain these results, image analysis already applied during our previous work [25] was used. The correlation was made between the data in the percentage of the clean part of the coating and void volume (Vv), a surface factor. This value was obtained from profilometric measurements and is measured in $\mu m^3/\mu m^2$ (see the detailed explanation in methods).

In Figure 11, the results about session 1 and 2 are reported. From Figure 11, it is possible to observe that the percentage of the clean part increases with void volume in both sessions.

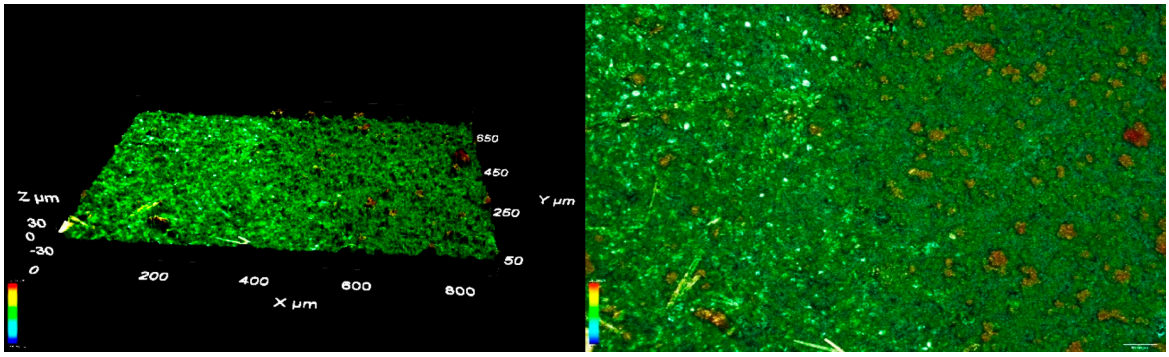

Figure 10. Three-dimensional (3D) and 2D images acquired by 3D profilometer on a sample portion. The right side underlying the bubble during immersion.

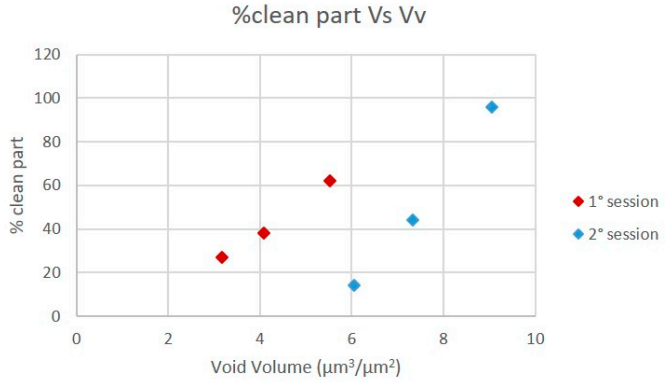

Figure 11. Cleaning efficiency as a function of void volume (Vv) parameters during the campaigns.

3.3. Corrosion

In Figure 12, the polarization curves of the SH electrodes achieved at the end of the two-month exposition period in natural seawater are depicted.

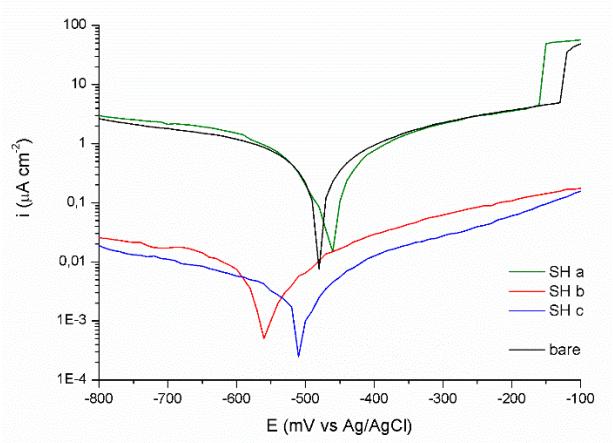

Figure 12. Polarization curves of aluminium electrodes covered with superhydrophobic coating after two months exposition in natural seawater. The samples were exposed, turning the SH surface to face the bottom of the tank.

Two behaviours can be distinguished. The first concerns the bare control, showing an $E_{(i)}$ curve featured by i_{corr} and $i_{pass} \approx 1$ µA/cm^{-2} and an $E_{pit} - E_{corr}$ passivity range broader than 300 mV, with $E_{corr} = -475$ mV versus Ref. Please check if these are correct. and $E_{pit} = -128$ mV versus Ref.

The second behaviour concerns the samples with SH treatment (SHb and SHc). Indeed, these samples exhibited lower i_{corr} and i_{pass} values and larger passivity potential range. With respect to

control, i_{corr} was lower by two orders of magnitude, while i_{pass} was lower by about 1.5 orders of magnitude. Regarding the potential passivity range, it has to be taken into account that the scan was stopped before the onset of pitting related phenomena leading to the polarization current rise in correspondence of E_{pit}. Although the upper limit was not detected in relation to the interruption of the polarization in correspondence of E_{int} = 0 mV versus Ref, with $E_{int} < E_{pit}$, the passivity potential window was in any case larger than controls.

Observing the curves coming from the SH coated samples, one curve (SHa) fairly resembled the behaviour of the control, exhibiting E_{corr} = −450 mV versus Ref., E_{pit} = −157 mV versus Ref., i_{corr}, and $i_{pass} \approx 1$ μA/cm^{-2}.

4. Discussion

4.1. Fouling and Bubble Formation

From these results, a possible bubble formation mechanism can be suggested. Under both surfaces (SHS and glass), the collected bubbles came from the seawater environment (gases dissolved in water), but the difference was that the SH coating was able to promote bubble nucleation and coalescence because of the presence of entrapped air between the asperity that characterized SHS. In fact, they are not adherent to the glass surface, as in the case of SH coatings.

These observations underline that the SH coating had a good adhesion with the glass substrate as long as it was not colonized by biofouling.

Despite a decrease of the roughness value, possibly owing to a slight loss of material, the water repellence of the coating remains unaltered (CA greater than 150° and hysteresis less than 5°).

Microscope analysis confirms that fouling inhibition was correlated to the ability of the surface to nucleate and keep adhering bubbles; the more homogeneous and bigger the bubbles, the better the fouling control of the surface. This behaviour appears to be dependent on surface roughness (*Sa*).

As reported in Figure 11, void volume seems to be a suitable parameter describing the extension of bubbles on the surfaces; this consideration is based on the fact that the void volume parameter indicates how much air would fill the surface (normalized to the measurement area) between the chosen material ratio values. The void volume measurements are derived from surface roughness parameter (*Sa*), as described in the work of [26].

Indeed, an SHS with high Vv better controlled the fouling evolution because of more air being trapped and generating a bigger air bubble shield, inhibiting the fouling growth. The two series (session 1—red dots and session 2—blue dots) well describe the fouling removability, even with differences probably due to an unpredictable loss of material during the cleaning procedure (session 1). As working curves, they allow us to find a more quantitative fouling removal efficiency as a compromise between a more probable loss of the SH properties at larger Vv and the percentage of removed fouling.

Nevertheless, as discussed [20], entrapped air is reduced in underwater conditions by the action of organic matter reaching the metal surface, with the result being the loss of the Cassie–Baxter state to the Wenzel state [27].

4.2. Corrosion

The electrochemical parameters deduced from the polarization curves clearly indicate that the SH coating investigated here can control corrosion phenomena. In particular, referring to bare electrode with no SH coating (control), the backward shift in SHb and SHc curves of both the anodic and cathodic branches reveal a mixed control of the corrosion phenomena.

The decrease of the corrosion current density of about two orders of magnitude is a result comparable to literature data evidencing corrosion protecting performances of SH coatings [15,27,28]. It is known that the corrosion protection afforded by SH coatings depends on the combined action of the coating itself and the air plastron entrapped within the texture of the SH coating surface [29–31]. Some

authors went inside this concern, evidencing the important role of trapped air as a dielectric inhibiting electron transfer between the electrolyte and the substrate [32]. This supplementary protection works as long as the air shield is present. In our case, the evidenced corrosion control included overall contributions of the coating and still resident bubbles. This result was achieved comparing by coated versus not coated electrodes tested at the end of the immersion time. For the future, additional information regarding the aging of the coating itself and the stability of the air plastron is needed. Indeed, both these components determine anticorrosion performances with complex mechanisms touching different connected variables, such as homogeneous/heterogeneous wetting degree of the interface; blockage of cathodic/anodic sites; and diffusion of crucial reactants such as Cl^-, O_2, and H^+ [32–34], whose dependence on time enhancing biological pressure can be expected.

The particular case of the SHa polarization curve indicates that the SH coating was not efficient In fact, for this sample, SH coating defects at the electrode–resin interface were observed, causing the electrode to work as the bare reference.

With the aim of fouling and corrosion control, the long-term stability in seawater of an SH coating deserves particular attention; indeed, this medium is characterized by biological pressure, given by the biofouling processes, and mechanical stresses, induced by water pressure, which potentially have a large impact on the SH coatings' protection performances [27].

Looking at the recent literature, the need to move towards real environment experimentation appears to be more and more evident. Previously cited authors' works, along with the works of [13,30,35,36], are precious in evidencing that SH coatings can be viewed as a promising and interesting solution for fouling and corrosion control, although results were obtained in model biological environments and in time windows less than a month. Concerning the approach to a real seawater environment, other authors [37,38] obtained noteworthy foul control results in a time window greater than a month. Hydrodynamic effects were investigated in a model environment with bacteria and diatoms up to 10 days [38]. The cited author investigated a lubricant layer evidencing the antagonistic role of the flow rate, able to induce foul release, but, in turn, threatening the stability of the layer per se. The stimulus coming from this work, although not dealing with the SH coating, is to think about the shear stress as a factor removing the air bubbles, determining the efficiency of the protection and, in this case, threatening the stability of the coating.

In relation to these aspects, our corrosion and foul control results were obtained in a time window extended up to two months in a full natural seawater environment, featuring all the stages of the biofouling processes (starting from the formation of the molecular conditioning film at $t < 1$–12 h). Encouraging results obtained in conservative conditions consist of a 180° turn of the SH surfaces with respect to sun facing and modest seawater turbulence, suggesting pushing further research efforts in testing the limits of SH performances environments with characteristics approaching those of the real seawater environments in which these coatings are actually demanded to work.

5. Conclusions

In this work, a sustainable solution for creating highly water repellent coatings with fouling control and anticorrosion properties in real seawater conditions was proposed. Starting from hydrophobic recyclable materials and utilizing a "green" solvent provides the potential for large-scale application of this option, owing to its low cost and ease to apply.

The results have shown that the superhydrophobicity can be obtained and maintained already at the micron scale with benefit towards the formation of a stable air plastron with the result of delaying the fouling formation and of an easy and high removability at a very low pressure.

The superhydrophobic coatings were applied on both glass and Al alloy substrate, and were tested in a real seawater environment with exposition up to two months, adopting conservative conditions consisting of a 180° tilt of the SH surfaces with respect to sun facing and low convection. This procedure was selected in the view of the progressive addition of the variables of a real seawater environment, in agreement with recent literature trends. Within this framework, our results are encouraging: fouling

was controlled by air bubbles' presence and corrosion current densities were two orders of magnitude lower than the control.

Further research should aim to determine whether the limits of the SH coating technology are compatible with limits imposed by applications in real seawater; coherently, time windows greater than months, full biological pressure, and different hydrodynamic conditions would still be determinant.

Author Contributions: Conceptualization, Project Administration, Funding Acquisition: M.F.; Investigation, Writing—Original Draft Preparation, Writing—Review and Editing: M.F., A.B. and F.C.

Funding: This research was funded by the Fondazione Bancaria Compagnia di San Paolo, Torino, ID ROL 20718, the Project ANFISOL-Design and the development of superamphiphobic coatings with self-cleaning properties for photovoltaic panels

Acknowledgments: M. Ferrari and F. Cirisano acknowledge the support of Fondazione Bancaria Compagnia di San Paolo, Torino. This work has been performed within the framework of the Project ANFISOL-Design and the development of superamphiphobic coatings with self-cleaning properties for photovoltaic panels (ID ROL 20718) funded by the Fondazione Bancaria Compagnia di San Paolo, Torino.

Conflicts of Interest: The authors declare no conflict of interest.

Nomenclature

E_{corr}	free corrosion potential
E_{pit}	free corrosion potential
E_{pit}	pitting potential
E_{int}	interruption potential
$R = E_{pit} - E_{corr}$	pitting resistance (or sensitivity)
i_{pass}	passivity current
Ref.	reference electrode

Appendix A

Table A1. Supporting information for Figure 6.

Bubble Diameters on the Samples	
Control	**SHS**
15% about 0.4 cm 85% < 0.2 cm	30% about 0.9 cm 20% about 0.5 cm 50% < 0.3 cm

References

1. Zhang, D.; Wang, L.; Qian, H.; Li, X. Superhydrophobic surfaces for corrosion protection: A review of recent progresses and future directions. *J. Coat. Technol. Res.* **2016**, *13*, 11–29. [CrossRef]
2. Montemor, M. Functional and smart coatings for corrosion protection: A review of recent advances. *Surf. Coat. Technol.* **2014**, *258*, 17–37. [CrossRef]
3. Huang, Y.; Huang, C.; Zhong, Y.; Yi, S. Preparing superhydrophobic surfaces with very low contact angle hysteresis. *Surf. Eng.* **2013**, *29*, 633–636. [CrossRef]
4. Yu, D.; Tian, J.; Dai, J.; Wang, X. Corrosion resistance of three-layer superhydrophobic composite coating on carbon steel in seawater. *Electrochim. Acta.* **2013**, *97*, 409–419. [CrossRef]
5. Zou, Y.; Wang, Y.; Xu, S.; Jin, T.; Wei, D.; Ouyang, J.; Jia, D.; Zhou, Y. Superhydrophobic double-layer coating for efficient heat dissipation and corrosion protection. *Chem. Eng. J.* **2019**, *362*, 638–649. [CrossRef]
6. Davis, J.R. The effects and economic impact of corrosion. In *Corrosion: Understanding the Basics*, 1st ed.; ASM International: Materials Park, OH, USA, 2000; pp. 1–21.
7. Xiang, T.; Han, Y.; Guo, Z.; Wang, R.; Zheng, S.; Li, S.; Li, C.; Dai, X. Fabrication of inherent anticorrosion superhydrophobic surfaces on metals. *ACS Sustain. Chem. Eng.* **2018**, *6*, 5598–5606. [CrossRef]

8. Zhang, B.; Zhu, Q.; Li, Y.; Hou, B. Facile fluorine-free one step fabrication of superhydrophobic aluminum surface towards self-cleaning and marine anticorrosion. *Chem. Eng. J.* **2018**, *352*, 625–633. [CrossRef]
9. Feng, L.; Yan, Z.; Qiang, X.; Liu, Y.; Wang, Y. Facile formation of superhydrophobic aluminum alloy surface and corrosion-resistant behavior. *Appl. Phys. A* **2016**, *122*, 165. [CrossRef]
10. Li, X.; Zhang, L.; Shi, T.; Zhang, C.; Zhang, L.C. Facile preparation of superhydrophobic structures on al alloys surfaces with superior corrosion resistance. *Mater. Corros.* **2019**, *70*, 558–565. [CrossRef]
11. Su, M.; Liu, Y.; Zhang, Y.; Wang, Z.; Li, Y.; He, P. Robust and underwater superoleophobic coating with excellent corrosion and biofouling resistance in harsh environments. *Appl. Surf. Sci.* **2018**, *436*, 152–161. [CrossRef]
12. Hassan, H.; Ismail, A.; Ahmad, S.; Soon, C. Super-hydrophobic green corrosion inhibitor on carbon steel. *Iop Conf. Ser. Mater. Sci. Eng.* **2017**, *215*, 012023. [CrossRef]
13. Selim, M.S.; Elmarakbi, A.; Azzam, A.M.; Shenashen, M.A.; EL-Saeed, A.M.; El-Safty, S.A. Eco-friendly design of superhydrophobic nano-magnetite/silicone composites for marine foul-release paints. *Prog. Org. Coat.* **2018**, *116*, 21–34. [CrossRef]
14. Shi, T.; Li, X.; Zhang, Q.; Li, B. One-step potentiostatic deposition of micro-particles on al alloy as superhydrophobic surface for enhanced corrosion resistance by reducing interfacial interactions. *Coatings* **2018**, *8*, 392. [CrossRef]
15. Qiu, Z.; Qiu, R.; Xiao, Y.; Zheng, J.; Lin, C. Slippery liquid-infused porous surface fabricated on cuzn: A barrier to abiotic seawater corrosion and microbiologically induced corrosion. *Appl. Surf. Sci.* **2018**, *457*, 468–476. [CrossRef]
16. Li, X.; Shi, T.; Li, B.; Zhang, C.; Zhong, B.; Lv, Y.; Zhang, Q. One-step preparation of super-hydrophobic micro-nano dendrites on al alloy for enhanced corrosion resistance. *Metals* **2018**, *8*, 960. [CrossRef]
17. Wen, G.; Huang, J.; Guo, Z. Energy-effective superhydrophobic nanocoating based on recycled eggshell. *Colloids Surf. A Phys. Eng. Asp.* **2019**, *568*, 20–28. [CrossRef]
18. Wong, H.S.; Barakat, R.; Alhilali, A.; Saleh, M.; Cheeseman, C.R. Hydrophobic concrete using waste paper sludge ash. *Cem. Concr. Res.* **2015**, *70*, 9–20. [CrossRef]
19. Ray, S.S.; Gandhi, M.; Chen, S.-S.; Chang, H.-M.; Dan, C.T.N.; Le, H.Q. Anti-wetting behaviour of a superhydrophobic octadecyltrimethoxysilane blended pvdf/recycled carbon black composite membrane for enhanced desalination. *Env. Sci. Water Res. Technol.* **2018**, *4*, 1612–1623. [CrossRef]
20. Benedetti, A.; Cirisano, F.; Delucchi, M.; Faimali, M.; Ferrari, M. Potentiodynamic study of Al–Mg alloy with superhydrophobic coating in photobiologically active/not active natural seawater. *Colloids Surf. B Biointerfaces* **2016**, *137*, 167–175. [CrossRef]
21. Liggieri, L.; Passerone, A. An automatic technique for measuring the surface tension of liquid metals. *High Temp. Technol.* **1989**, *7*, 82–86. [CrossRef]
22. *ISO 25178-2:2012 Geometrical Product Specifications (GPS)—Surface Texture: Areal—Part 2: Terms, Definitions and Surface Texture Parameters*; The International Organization for Standardization: Geneva, Switzerland, 2012.
23. Cassie, A.B.D.; Baxter, S. Wettability of porous surfaces. *Trans. Faraday Soc.* **1944**, *40*, 546–551. [CrossRef]
24. Ferrari, M.; Cirisano, F. Hydrophobicity and superhydrophobicity in fouling prevention in sea environment. In *Advances in Contact Angle, Wettablility and Adhesion*; Mittal, K.L., Ed.; John Wiley & Sons: Newark, NJ, USA, 2018; pp. 241–265.
25. Cirisano, F.; Benedetti, A.; Liggieri, L.; Ravera, F.; Santini, E.; Ferrari, M. Amphiphobic coatings for antifouling in marine environment. *Colloids Surf. A Physicochem. Eng. Asp.* **2016**, *505*, 158–164. [CrossRef]
26. Blateyron, F. The areal field parameters. In *Characterisation of Areal Surface Texture*; Springer: Berlin Heidelberg, Germany, 2013; pp. 15–43.
27. Ferrari, M.; Benedetti, A. Superhydrophobic surfaces for applications in seawater. *Adv. Colloid Interface Sci.* **2015**, *222*, 291–304. [CrossRef] [PubMed]
28. Xu, W.; Song, J.; Sun, J.; Lu, Y.; Yu, Z. Rapid fabrication of large-area, corrosion-resistant superhydrophobic mg alloy surfaces. *ACS Appl. Mater. Interfaces* **2011**, *3*, 4404–4414. [CrossRef]
29. Wan, Y.; Chen, M.; Liu, W.; Shen, X.; Min, Y.; Xu, Q. The research on preparation of superhydrophobic surfaces of pure copper by hydrothermal method and its corrosion resistance. *Electrochim. Acta* **2018**, *270*, 310–318. [CrossRef]

30. Zhang, B.; Hu, X.; Zhu, Q.; Wang, X.; Zhao, X.; Sun, C.; Li, Y.; Hou, B. Controllable Dianthus caryophyllus-like superhydrophilic/superhydrophobic hierarchical structure based on self-congregated nanowires for corrosion inhibition and biofouling mitigation. *Chem. Eng. J.* **2017**, *312*, 317–327. [CrossRef]
31. Liu, T.; Chen, S.; Cheng, S.; Tian, J.; Chang, X.; Yin, Y. Corrosion behavior of super-hydrophobic surface on copper in seawater. *Electrochim. Acta* **2007**, *52*, 8003–8007. [CrossRef]
32. Wang, P.; Zhang, D.; Qiu, R.; Hou, B. Super-hydrophobic film prepared on zinc as corrosion barrier. *Corros. Sci.* **2011**, *53*, 2080–2086. [CrossRef]
33. Boinovich, L.B.; Emelyanenko, A.M.; Modestov, A.D.; Domantovsky, A.G.; Emelyanenko, K.A. Not simply repel water: The diversified nature of corrosion protection by superhydrophobic coatings. *Mendeleev Commun.* **2017**, *27*, 254–256. [CrossRef]
34. Boinovich, L.B.; Emelyanenko, A.M.; Modestov, A.D.; Domantovsky, A.G.; Shiryaev, A.; Emelyanenko, K.A.; Dvoretskaya, O.; Ganne, A. Corrosion behavior of superhydrophobic aluminum alloy in concentrated potassium halide solutions: When the specific anion effect is manifested. *Corros. Sci.* **2016**, *112*, 517–527. [CrossRef]
35. Cho, E.-C.; Chang-Jian, C.-W.; Chen, H.-C.; Chuang, K.-S.; Zheng, J.-H.; Hsiao, Y.-S.; Lee, K.-C.; Huang, J.-H. Robust multifunctional superhydrophobic coatings with enhanced water/oil separation, self-cleaning, anti-corrosion, and anti-biological adhesion. *Chem. Eng. J.* **2017**, *314*, 347–357. [CrossRef]
36. He, X.; Cao, P.; Tian, F.; Bai, X.; Yuan, C. Autoclaving-induced in-situ grown hierarchical structures for construction of superhydrophobic surfaces: A new route to fabricate antifouling coatings. *Surf. Coat. Technol.* **2019**, *357*, 180–188. [CrossRef]
37. Selim, M.S.; Yang, H.; Wang, F.Q.; Fatthallah, N.A.; Huang, Y.; Kuga, S. Silicone/zno nanorod composite coating as a marine antifouling surface. *Appl. Surf. Sci.* **2019**, *466*, 40–50. [CrossRef]
38. Wang, P.; Zhang, D.; Sun, S.; Li, T.; Sun, Y. Fabrication of slippery lubricant-infused porous surface with high underwater transparency for the control of marine biofouling. *ACS Appl. Mater. Interfaces* **2016**, *9*, 972–982. [CrossRef]